




Chiral and nonreciprocal transmission of single photons in coupled-resonator-waveguide systemsJun-Cong Zheng, Xing-Liang Dong, Jia-Qiang Chen, Xin-Lei Hei , Xue-Feng Pan, Xiao-Yu Yao ,
Yu-Meng Ren, Yi-Fan Qiao, and Peng-Bo Li **Ministry of Education Key Laboratory for Nonequilibrium Synthesis and Modulation of Condensed Matter, Shaanxi Province Key Laboratory of Quantum Information and Quantum Optoelectronic Devices, School of Physics, Xi'an Jiaotong University, Xi'an 710049, China*

(Received 27 February 2024; revised 15 May 2024; accepted 3 June 2024; published 24 June 2024)

In this paper, we employ two two-level atoms and a Λ -type atom to connect two one-dimensional semi-infinite coupled resonator waveguides, respectively. The first configuration is a chiral setup, where incident photons undergo an elastic scattering process. We investigate the influence on the single-photon transfer rate of spatial coupling points between the small or giant atom and the waveguides. Our numerical simulations demonstrate that additional coupling points in the giant atom system will modify the transmission rule observed in the small atom system due to their unique interference effects. The second configuration is a nonreciprocal setup, where the conduction direction depends entirely on the initial state of the Λ -type atom. The incident photon undergoes an inelastic scattering process accompanied by frequency conversion.

DOI: [10.1103/PhysRevA.109.063709](https://doi.org/10.1103/PhysRevA.109.063709)**I. INTRODUCTION**

Quantum information science, as an essential topic in quantum optics, optomechanical systems [1–3], cold atom physics [4–6], cavity quantum electrodynamics (cavity QED) systems [7–9], and superconducting circuit quantum electrodynamics (circuit QED) systems [10–12], has been proposed to obtain and transport quantum information through the interaction between light and matter. To expand the physical space of transmission, waveguide QED has recently garnered considerable attention [13–16]. For instance, the coupled resonator waveguide (CRW) [17–20] has been widely studied in quantum routers [21], quantum memories [22], and slow light applications [23]. Compared with traditional continuous waveguides, CRW offers several advantages, such as tunable group velocity for traveling photons [24], control over the dissipation or decoherence of atoms [25], and the ability to induce effective coupling between remote atoms [26].

In the traditional atom-CRW scheme, the dipole approximation is typically invoked [27], treating the atom as a pointlike object that only interacts with the waveguide at a single resonator. However, the dipole approximation becomes inadequate when the size of the atom becomes comparable or larger than the mode wavelength. In such cases, the atom interacts with the CRW at multiple coupling points, and the atom is referred to as a giant atom [28,29]. Generally, giant atoms can be achieved by increasing the ratio between the atomic size and the mode wavelength [30–32] or by coupling a small atom to the curved waveguide at well-separated locations [33,34]. The distinctive configurations of these structures lead to physical phenomena distinct from those observed in small atom systems. This distinction arises from the phase differences resulting from parametric couplings and direction-dependent phase delays, encompassing effects such

as time delay [35,36], decoherence-free interaction among giant atoms [37,38], photon storage [39,40], and beyond.

Different configurations of the atom-CRW usually correspond to different functions; examples include chiral and nonreciprocal setups. The latter, such as diodes [41–48], and circulators [49–53], have been widely studied for their usefulness. In this work, we construct two types of atom-CRW systems, involving either small or giant atoms, to achieve single-photon chiral and nonreciprocal transmission, respectively. The first system consists of two one-dimensional (1D) semi-infinite CRWs connected by two coupled two-level atoms. The transmission of a single photon is not affected by the incident port, undergoing an elastic scattering process. Our numerical simulations show that the transfer rate of the incident photon can be changed by adjusting the coupling point between atoms and waveguides. Moreover, the second coupling point for each giant atom can alter the transport laws in small atomic systems. In the second setup, similar to the configuration described in Ref. [54], we employ a Λ -type atom coupled to the CRWs, collectively forming a nonreciprocal device. The unidirectional transmission of a single photon is contingent upon the initial state of the atom, involving an inelastic scattering process that leads to the frequency conversion of the incident photon, which differs from the mechanism observed in chiral-giant-molecule waveguide systems [55]. We investigate the impact of coupling points on the transfer rate at resonance, and intriguingly, the observed peculiarity mirrors that of the scenario with two two-level atoms. Lastly, we delve into the influence of three distinct CRW band configurations on both the reflectance and transfer rate.

This work is structured as follows. In Sec. II, we introduce the model of a two two-level atom system and present the corresponding Hamiltonian. The analysis of the single-photon scattering process for the small atom system is presented in Sec. II A, while Sec. II B delves into the same process for the giant atom system. Moving on to Sec. III, we substitute the two two-level atoms from Sec. II with a Λ -type atom and explore the single-photon scattering process for both small and

*Contact author: lipengbo@mail.xjtu.edu.cn

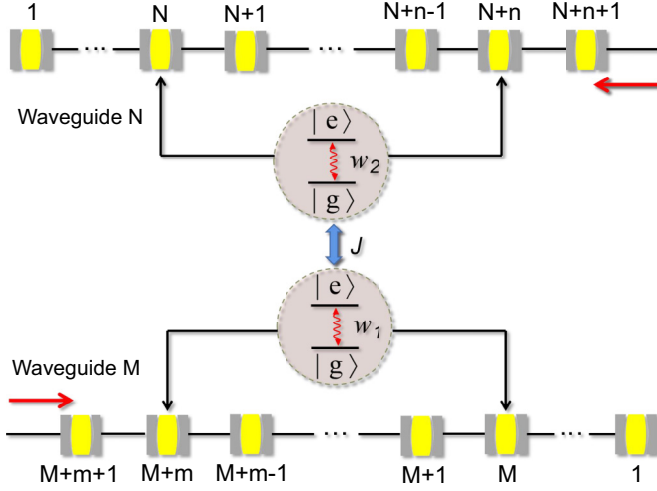


FIG. 1. The system comprises a semi-infinite coupled resonator waveguide, referred to as the lower bus waveguide M , and a semi-infinite coupled resonator waveguide, referred to as the upper drop waveguide N . These waveguides are interconnected by a molecule at four resonators ($M, M+m, N, N+n$), respectively. The molecule consists of two interacting two-level atoms with a coupling strength denoted as J .

giant atom cases. Additionally, we investigate the impact of three distinct configurations of CRW bands on single-photon transmission. Section IV is dedicated to a discussion on the experimental feasibility, and finally, Sec. V provides a summary of the findings.

II. CHIRAL TRANSMISSION OF SINGLE PHOTONS WITH TWO TWO-LEVEL ATOMS

Our proposed system comprises two semi-infinite CRWs, each forming a quasi-1D array of identical optical cavities with nearest-neighbor coupling. The connection between these two CRWs is established by a molecule (refer to Fig. 1). The first two-level atom, characterized by the transition frequency ω_1 between the ground state $|g\rangle$ and the excited state $|e\rangle$, is coupled to CRW- M at resonator M and resonator $M+m$ with the coupling strength g_1 . The second atom, with the transition frequency ω_2 , is coupled to CRW- N at resonator N and resonator $N+n$ with the coupling strength g_2 . The interaction between these two atoms is governed by the coupling strength J , mediated through virtual photon exchange [56].

A. Small atom system in the case of $m = n = 0$

When we set $m = n = 0$, the initial two coupling points converge into a singular coupling point. In this arrangement, there is the small atoms couple with the waveguide at individual resonators, and the system's Hamiltonian can be represented as (assuming $\hbar = 1$).

$$H_1 = H_a + H_w + H_{\text{int}},$$

$$H_a = \sum_{i=1}^2 \omega_i \sigma_i^+ \sigma_i^-,$$

$$H_w = \sum_{\alpha=M,N} \left\{ \omega_\alpha \sum_j a_\alpha^\dagger(j) a_\alpha(j) \right.$$

$$\left. - \xi_\alpha \sum_{j=1}^{+\infty} [a_\alpha^\dagger(j+1) a_\alpha(j) + a_\alpha^\dagger(j) a_\alpha(j+1)] \right\},$$

$$H_{\text{int}} = g_1 a_M^\dagger(M) \sigma_1^- + g_2 a_N^\dagger(N) \sigma_2^- + J \sigma_1^- \sigma_2^+ + \text{H.c.} \quad (1)$$

Here, H_a represents the free Hamiltonian of the atoms, and σ_i^+ (σ_i^-) denotes the raising (lowering) operator of the atom. H_w is the Hamiltonian for the CRWs with the homogeneous intercavity coupling constant ξ_α . The operators $a_\alpha^\dagger(j)$ (where $j = 1, \dots, +\infty$) represent the creation operator of the j th single-mode resonator with frequency ω_α for the waveguide α . The term H_{int} comprises two parts: (i) the interactions between the atomic transitions and the CRWs, and (ii) an effective atom-atom coupling.

H_w describes the typical tight-binding boson model, where each CRW possesses an energy band centered at ω_α with a bandwidth of $4\xi_\alpha$. The chosen frequency ω_α allows the dispersion relation of the waveguide to be linearized as $E_M = \omega_M - 2\xi_M \cos(k)$ and $E_N = \omega_N - 2\xi_N \cos(q)$ [21,57]. Here, k and q represent the wave vectors of the propagating single photon in CRW- M and CRW- N , respectively. For simplicity, we assume $\xi_M = \xi_N = \xi$, $g_1 = g_2 = J = g$ in the following discussion. Initially, we prepare two atoms in the ground state $|g\rangle$, and a single photon can be incident from either the infinitely far left end of CRW- M or the infinitely far right end of CRW- N . Following elastic scattering between the atom and the photon, the eigenvalue of each waveguide remains unchanged (i.e., $E_M = E_N$). Assuming $\omega_M = \omega_N$, we have $k = q$.

In this section, we delve into the single-photon scattering process. This can be elucidated by expressing the single-excitation eigenstate as

$$|\psi\rangle = \left\{ \sum_j [c_M(j) a_M^\dagger(j) + c_N(j) a_N^\dagger(j)] + \sum_{i=1}^2 u_{ei} \sigma_i^+ \right\} |\emptyset\rangle, \quad (2)$$

$|\emptyset\rangle$ represents the vacuum state of the resonator field, while the atoms are in the ground state $|g\rangle$. $c_M(j)$ and $c_N(j)$ denote the probability amplitudes for finding a photonic excitation in resonator j of CRW- M and CRW- N , respectively. u_{ei} stands for the excitation amplitude of the atom.

We derive the coupled stationary equations for the amplitudes from the eigenvalue equation $H_1 |\psi\rangle = E |\psi\rangle$

$$(E - \omega_M) c_M(M) = -\xi [c_M(M-1) + c_M(M+1)] + g u_{e1}, \quad (3a)$$

$$(E - \omega_N) c_N(N) = -\xi [c_N(N-1) + c_N(N+1)] + g u_{e2}, \quad (3b)$$

$$(E - \omega_1) u_{e1} = g [c_M(M) + u_{e2}], \quad (3c)$$

$$(E - \omega_2) u_{e2} = g [c_N(N) + u_{e1}]. \quad (3d)$$

First, we consider a scenario where a single photon with wave vector k is incident from the left side of CRW- M , and the atoms occupy the state $|g\rangle$. In the regime $j > M$, both incident and reflected photons coexist, while in the regime $j > N$, only the transmitted photon exists. For $j \leq M$ or $j \leq N$, the boundary compels the photon to be generated as a stationary

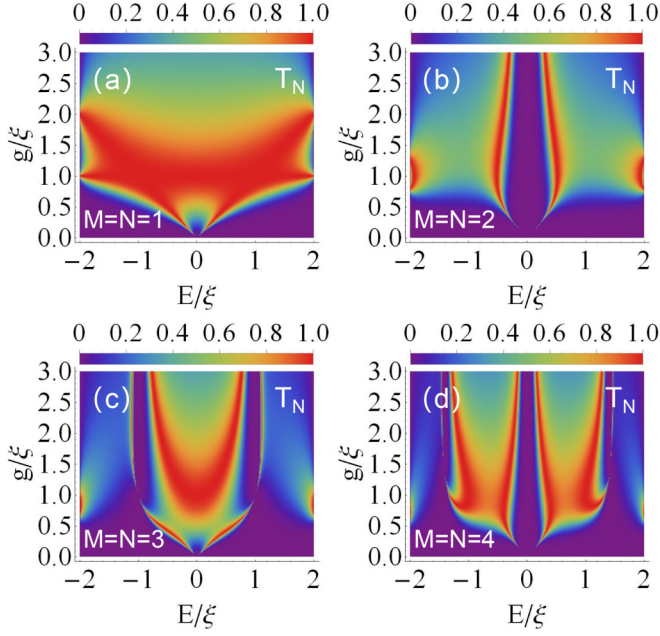


FIG. 2. The spectra of the single-photon transfer rate T_N are plotted as functions of the incident energy E and the coupling strength g . In (a), we consider $M = N = 1$; in (b), $M = N = 2$; in (c), $M = N = 3$; and in (d), $M = N = 4$. These spectra are calculated for the parameter values $\omega_M = \omega_N = \omega_1 = \omega_2 = 0$.

wave within the finite CRWs. Therefore, the wave functions in the asymptotic regions are given, respectively, by

$$c_M(j) = \begin{cases} e^{-ikj} + r_M e^{ikj}, & j > M \\ A \sin(kj), & j = 1, 2, \dots, M \end{cases} \quad (4)$$

and

$$c_N(j) = \begin{cases} t_N e^{iqj}, & j > N \\ B \sin(qj), & j = 1, 2, \dots, N \end{cases} \quad (5)$$

where r_M is the reflected amplitude in CRW- M , and t_N is the transfer amplitude in CRW- N . The corresponding continuity conditions at $j = M, N$ are

$$e^{-ikM} + r_M e^{ikM} = A \sin(kM), \quad (6a)$$

$$t_N e^{iqN} = B \sin(qN). \quad (6b)$$

Taking the simplest case as an example, we choose $M = N = 1$ and assume $\omega_M = \omega_N = \omega_1 = \omega_2 = 0$ [58]. By applying solutions (4) and (5) to the discrete scattering equations (3), we obtain the transfer amplitude,

$$t_N = \frac{e^{-3ik}(e^{2ik} - 1)g^3\xi}{\eta + 2Ee^{ik}(E^2 - 2g^2)\xi + e^{2ik}(E^2 - g^2)\xi^2}, \quad (7)$$

where $\eta = E^4 - 3E^2g^2 + g^4$.

In Fig. 2, we have illustrated the transfer rate $T_N = |t_N|^2$ as a function of both the incident energy E and the coupling strength g for various atom-CRW configurations with $M = N = 1, 2, 3, 4$. Figure 2(a) reveals that, within a broad bandwidth, high transfer rates are predominantly concentrated in

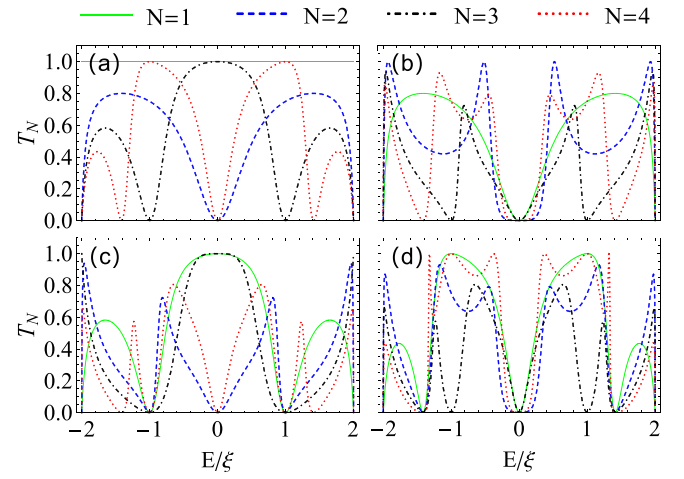


FIG. 3. The spectra of the single-photon transfer rate T_N are plotted as functions of the incident energy E . In (a), we consider $M = 1$; in (b), $M = 2$; in (c), $M = 3$; and in (d), $M = 4$. Each group of spectra corresponds to four different values of N , where $N = 1$ (solid green line), $N = 2$ (blue dashed line), $N = 3$ (black dot-dashed line), and $N = 4$ (red dashed line). These spectra are calculated for the parameters $g = 1\xi$, $\omega_M = \omega_N = \omega_1 = \omega_2 = 0$.

the range $g \in [1\xi, 1.5\xi]$. Notably, when the coupling strength g equals the intercavity coupling constant ξ , the transfer rate T_N attains unity across the entire bandwidth. This behavior can be analytically verified by applying the dispersion relation $E = 2\xi \cos(k)$ to the transfer amplitude (7). Figures 2(b) and 2(d) depict scenarios where both M and N are even values. In these cases, incident photons are completely reflected near the band center ($E = 0$), and this outcome remains independent of the coupling strength.

To further investigate the relationship between coupling position and transfer amplitude, we depict the spectra of the single-photon transfer rate T_N as a function of the incident energy E in Fig. 3 for various combinations of M and N . The system operates symmetrically, as evidenced by the coincidence of the T_N curve for $M = 1, N = 3$ (black dot-dashed line) in Fig. 3(a) and $M = 3, N = 1$ (solid green line) in Fig. 3(c). We further validate this symmetry in the ensuing discussion. In Fig. 3(a) with $N = 1$, the curve manifests as a flat band with $T_N = 1$ throughout the entire bandwidth, aligning with the results in Fig. 2(a). Focusing on the discrepancy near $E = 0$, it is observed that single-photon transfer occurs exclusively when either $M = N = 1$ or $M = 1, N = 3$ in Fig. 3(a), and $M = 3, N = 1$ or $M = N = 3$ in Fig. 3(c). A comparative analysis of all 16 curves suggests that achieving $T_N \approx 1$ at resonance is possible only when both M and N are odd values. Additionally, we note that the bandwidth of high transfer rate is broader when the sum of the number M and N is smaller.

In superconducting quantum devices, Josephson junction loops threaded by external fluxes allow us to introduce a local coupling phase [59], represented by θ , which induces intriguing interference effects in the scattering properties. The atom-CRW coupling is described as $g_1 = g_2 = ge^{i\theta}$. In Fig. 4, we compare the cases where $\theta = \pi$ and $\theta = \pi/2$. We observe that the additional coupling phase does not significantly

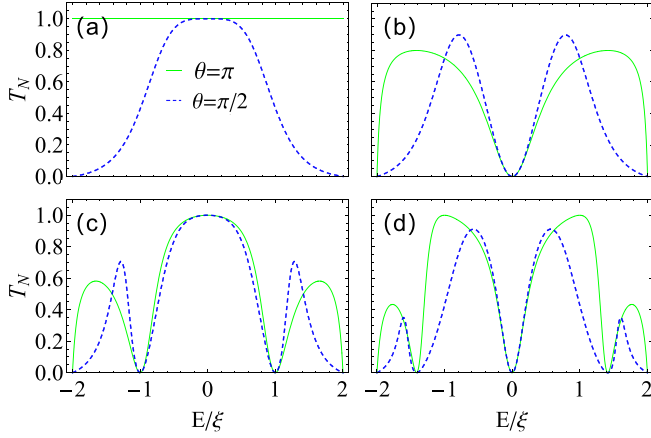


FIG. 4. The spectra of the single-photon transfer rate T_N are plotted as functions of the incident energy E . In (a), we consider $N = 1$; in (b), $N = 2$; in (c), $N = 3$; and in (d), $N = 4$. Each group of spectra corresponds to two different values of θ , where $\theta = \pi$ (solid green line), $\theta = \pi/2$ (blue dashed line). These spectra are calculated for the parameters $g = 1\xi$, $\omega_M = \omega_N = \omega_1 = \omega_2 = 0$, $M = 1$.

affect the transmission rule at resonance. However, outside the resonance region, the transfer rate T_N undergoes a noticeable change, especially at $M = N = 1$, where the flat band characterized by $T_N = 1$ is significantly reduced. Hence, it becomes feasible to manipulate single-photon scattering through an external field.

Now, let us consider another scenario where a single photon with wave vector q is incident from the right side of CRW- N , and the atoms occupy the state $|g\rangle$. The wave functions in the asymptotic regions are given, respectively, by

$$\tilde{c}_M(j) = \begin{cases} \tilde{t}_M e^{ikj}, & j > M \\ \tilde{B} \sin(kj), & j = 1, 2, \dots, M \end{cases} \quad (8)$$

and

$$\tilde{c}_N(j) = \begin{cases} e^{-iqj} + \tilde{r}_N e^{iqj}, & j > N \\ \tilde{A} \sin(qj), & j = 1, 2, \dots, N \end{cases} \quad (9)$$

where \tilde{t}_M is the transfer amplitude in CRW- M , and \tilde{r}_N is the reflected amplitude in CRW- N . The corresponding continuity conditions at $j = M, N$ are

$$\tilde{t}_M e^{ikM} = \tilde{B} \sin(kM), \quad (10a)$$

$$e^{-iqN} + \tilde{r}_N e^{iqN} = \tilde{A} \sin(qN). \quad (10b)$$

It can be demonstrated that there always exist $t_N = \tilde{t}_M$ and $r_N = \tilde{r}_M$ in the scattering process. The entry direction does not influence the transfer rate of the single photon. Therefore, the operation of this device exhibits chirality. Moreover, by selecting $\omega_M = \omega_1$ and $\omega_N = \omega_2$, it becomes feasible to effectively connect two waveguides with different center frequencies. This achievement contrasts with the single-atom scenario, where a substantial detuning between the atom and the waveguide is encountered, as discussed in Ref. [60].

B. Giant atom system in the case of $m \neq 0$ or $n \neq 0$

Now, we replace the small atoms in Sec. II A with giant atoms ($m \neq 0$ or $n \neq 0$). Each giant atom is coupled to the waveguide at two resonators. The related parameters are consistent with those in Sec. II A. The novel interaction Hamiltonian is expressed as

$$H'_{\text{int}} = g[a_M^\dagger(M) + a_M^\dagger(M+m)]\sigma_1^- + g[a_N^\dagger(N) + a_N^\dagger(N+n)]\sigma_2^- + g\sigma_1^-\sigma_2^+ + \text{H.c.}, \quad (11)$$

and we have the Hamiltonian of the whole system $H_2 = H_a + H_w + H'_{\text{int}}$.

We obtain the coupled stationary equations for the amplitudes from the eigenvalue equation $H_2|\psi\rangle = E|\psi\rangle$

$$(E - \omega_M)c_M(M) = -\xi[c_M(M-1) + c_M(M+1)] + gu_{e1}, \quad (12a)$$

$$(E - \omega_M)c_M(M+m) = -\xi[c_M(M+m-1) + c_M(M+m+1)] + gu_{e1}, \quad (12b)$$

$$(E - \omega_N)c_N(N) = -\xi[c_N(N-1) + c_N(N+1)] + gu_{e2}, \quad (12c)$$

$$(E - \omega_N)c_N(N+n) = -\xi[c_N(N+n-1) + c_N(N+n+1)] + gu_{e2}, \quad (12d)$$

$$(E - \omega_1)u_{e1} = g[c_M(M) + c_M(M+m) + u_{e2}], \quad (12e)$$

$$(E - \omega_2)u_{e2} = g[c_N(N) + c_N(N+n) + u_{e1}]. \quad (12f)$$

We consider a scenario in which a single photon with wave vector k is incident from the left side of CRW- M , and the atoms occupy the state $|g\rangle$. Unlike the small atomic system, there are simultaneously plane waves moving in opposite directions in the regime $M < j \leq M+m$ or $N < j \leq N+n$. Therefore, the wave functions in the asymptotic regions are given, respectively, by

$$c_M(j) = \begin{cases} e^{-ikj} + r_M e^{ikj}, & j > M+m \\ C e^{ikj} + D e^{-ikj}, & M < j \leq M+m \\ A \sin(kj), & j = 1, 2, \dots, M \end{cases} \quad (13)$$

and

$$c_N(j) = \begin{cases} t_N e^{iqj}, & j > N+n \\ E e^{iqj} + F e^{-iqj}, & N < j \leq N+n \\ B \sin(qj), & j = 1, 2, \dots, N \end{cases} \quad (14)$$

Together with the continuous condition at $j = \{M, M+m, N, N+n\}$, which are

$$e^{-ik(M+m)} + r_M e^{ik(M+m)} = C e^{ik(M+m)} + D e^{-ik(M+m)}, \quad (15a)$$

$$C e^{ikM} + D e^{-ikM} = A \sin(kM), \quad (15b)$$

$$t_N e^{iq(N+n)} = E e^{iq(N+n)} + F e^{-iq(N+n)}, \quad (15c)$$

$$E e^{iqN} + F e^{-iqN} = B \sin(qN). \quad (15d)$$

By applying solutions (13) and (14) to the discrete scattering equations (12), the transfer amplitude t_N and the reflected amplitude r_M can be obtained.

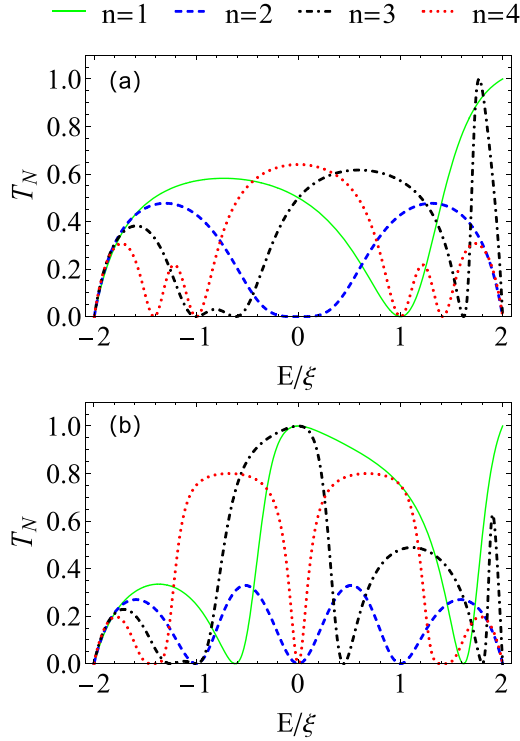


FIG. 5. The single-photon transfer rate T_N spectra are plotted as functions of the incident energy E for the case of $M = N = 1$ in (a) and $M = 1, N = 2$ in (b). Each group of spectra corresponds to four different values of n , where $n = 1$ (solid green line), $n = 2$ (blue dashed line), $n = 3$ (black dot-dashed line), and $n = 4$ (red dashed line). These spectra are calculated for the parameters $g = 1\xi$, $\omega_M = \omega_N = \omega_1 = \omega_2 = 0$, $m = 0$.

We investigate the effect of the size of the giant atom on the transfer rate T_N in Fig. 5. We choose $m = 0$ and select the value of n from 1 to 4, meaning the molecule is asymmetric, with the upper part being a giant atom and the lower part being a small atom. Figure 5(a) corresponds to the case shown in Fig. 3(a) by the green solid line, where $M = N = 1$. It manifests that the additional coupling point has an obvious effect on single-photon transmission due to the unique interference effects. For instance, $T_N < 0.7$ in the whole bandwidth when n is even, and only a single eigenenergy point at the edge satisfies $T_N = 1$ when n is odd. Figure 5(b) corresponds to the case shown in Fig. 3(a) by the blue dashed line, where $M = 1, N = 2$. Around $E = 0$, the small atom system acts as a mirror, blocking the propagation of photons [61–64], while the giant atom system allows the incident photon to be transferred by selecting odd values for n .

In Fig. 6, the molecule comprises two giant atoms ($m = n = 1$) and exhibits symmetry. Under this configuration, we consistently assume $M = N$ and systematically investigate the impact on the transfer rate T_N with simultaneous increments in the values of M and N . The curve in Fig. 6 for $M = N = 1$ corresponds to the cases depicted in Fig. 3(a) by the green solid line; $M = N = 2$ corresponds to the cases shown in Fig. 3(b) by the blue dashed line; $M = N = 3$ corresponds to the cases illustrated in Fig. 3(c) by the black dot-dashed line; and $M = N = 4$ corresponds to the instances presented

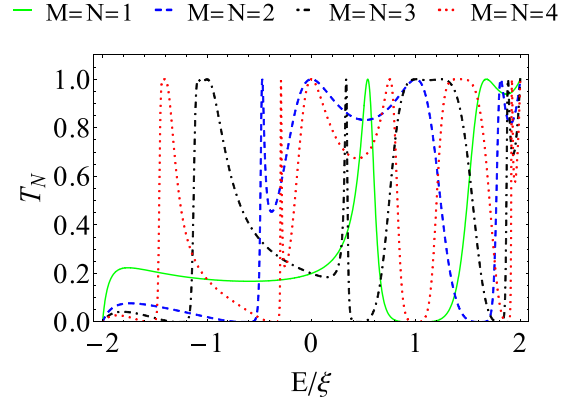


FIG. 6. The single-photon transfer rate T_N spectrum is plotted as a function of the incident energy E . There are four different values of M and N , where $M = N = 1$ (solid green line), $M = N = 2$ (blue dashed line), $M = N = 3$ (black dot-dashed line), and $M = N = 4$ (red dashed line). The spectrum is calculated for the parameters $g = 1\xi$, $\omega_M = \omega_N = \omega_1 = \omega_2 = 0$, $m = n = 1$.

in Fig. 3(d) by the red dashed line. Upon comparing these four sets of curves around $E = 0$, it becomes evident that, akin to the scenario with a single giant atom, the additional coupling points of two giant atoms can effectively govern the transmission of incident photons. Specifically, they can facilitate the opening of closed CRWs when M and N are even values. Conversely, they significantly diminish the transfer rate for the opened CRWs when M and N are odd values. Furthermore, owing to the distinctive interference effects between the two coupling points of giant atoms, the symmetry of the spectrum is disrupted, resulting in a more disordered pattern.

III. SINGLE-PHOTON NONRECIPROCAL TRANSMISSION WITH A Λ -TYPE ATOM

In this section, we replace the two two-level atoms in Sec. II with a Λ -type atom, as depicted in Fig. 7. The

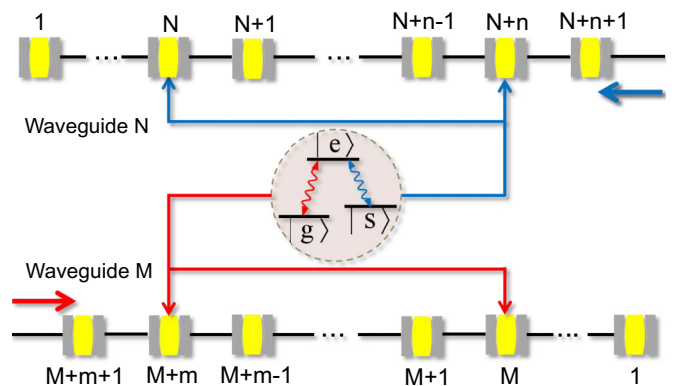


FIG. 7. The system consists of a semi-infinite coupled resonator waveguide, denoted as the lower bus waveguide M , and a semi-infinite coupled resonator waveguide, denoted as the upper drop waveguide N . These waveguides are connected by a Λ -type atom at four resonators ($M, M + m, N, N + n$), respectively. The atomic transitions $|g\rangle \leftrightarrow |e\rangle$ coupled to CRW- M (red line) and $|s\rangle \leftrightarrow |e\rangle$ coupled to CRW- N (blue line).

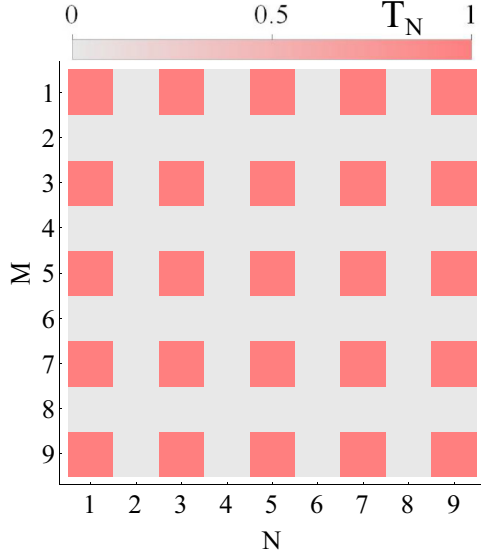


FIG. 8. The single-photon transfer rate T_N spectrum is plotted as functions of M and N . The spectrum is calculated for the parameter $\omega_M = \omega_e = 0$, $g_1 = g_2 = g = 1\xi$.

Λ -type atom possesses atomic transitions $|g\rangle \leftrightarrow |e\rangle$ coupled to CRW- M and $|s\rangle \leftrightarrow |e\rangle$ coupled to CRW- N , respectively. This atom-waveguide coupling form is similar to that in Ref. [65].

The setup functions akin to a diode, where the permissible direction for the single photon's travel hinges on the initial state of the atom. Initially, we prepare the atom in state $|g\rangle$. Let us envision a single photon with wave vector k approaching from the left side of CRW- M . Upon interacting with the atom, the incident photon can be redirected to CRW- N via frequency conversion $k \rightarrow q$. This process involves inelastic scattering, inducing a change in waveguide energy $\Delta = E_N - E_M = -\omega_s$. However, if the same photon arrives from the right side of CRW- N , it won't be absorbed due to the atomic transition $|s\rangle \leftrightarrow |e\rangle$. Next, we prepare the atom in state $|s\rangle$. This state facilitates the single photon's journey from CRW- N to CRW- M through frequency conversion $k' \rightarrow q'$, with an energy shift between waveguides of $\Delta' = E_M - E_N = \omega_s$. To summarize, this setup enables single-photon nonreciprocal transmission with frequency conversion, where the direction of conduction is entirely dictated by the initial state of the atom.

The Hamiltonian of the small atom system can be written as (setting $\hbar = 1$)

$$\begin{aligned} \tilde{H} &= \tilde{H}_a + \tilde{H}_w + \tilde{H}_{\text{int}}, \\ \tilde{H}_a &= \omega_e \sigma_g^+ \sigma_g^- + \omega_s \sigma_s^- \sigma_s^+, \\ \tilde{H}_w &= \sum_{\alpha=M,N} \left\{ \omega_\alpha \sum_j a_\alpha^\dagger(j) a_\alpha(j) \right. \\ &\quad \left. - \xi_\alpha \sum_{j=1}^{+\infty} [a_\alpha^\dagger(j+1) a_\alpha(j) + a_\alpha^\dagger(j) a_\alpha(j+1)] \right\}, \\ \tilde{H}_{\text{int}} &= g a_M^\dagger(M) \sigma_g^- + g a_N^\dagger(N) \sigma_s^- + \text{H.c.}, \end{aligned} \quad (16)$$

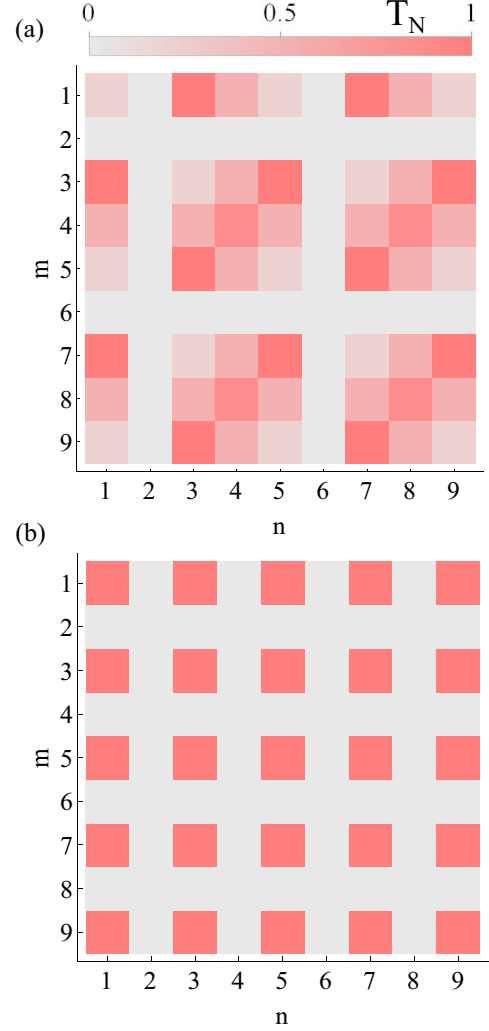


FIG. 9. The single-photon transfer rate T_N spectra are plotted as functions of m and n for the case of $M=N=1$ in (a) and $M=N=2$ in (b). These spectra are calculated for the parameter $\omega_M = \omega_e = 0$, $g_1 = g_2 = g = 1\xi$.

where $\sigma_g^+ = |e\rangle\langle g|$ and $\sigma_s^+ = |e\rangle\langle s|$ are the raising operators of the atom. ω_e and ω_s are the energies of the states $|e\rangle$ and $|s\rangle$ with respect to the state $|g\rangle$, respectively.

The single excitation eigenstate for this system by expressing as

$$|\tilde{\psi}\rangle = \left\{ \sum_j [c_M(j) a_M^\dagger(j) + c_N(j) a_N^\dagger(j)] + u_e (\sigma_g^+ + \sigma_s^+) \right\} |\emptyset\rangle. \quad (17)$$

We obtain the coupled stationary equations of small atom system for the amplitudes as

$$(E - \omega_M) c_M(M) = -\xi [c_M(M-1) + c_M(M+1)] + g u_e, \quad (18a)$$

$$(E - \omega_N - \omega_s) c_N(N) = -\xi [c_N(N-1) + c_N(N+1)] + g u_e, \quad (18b)$$

$$(E - \omega_e) u_e = g c_M(M) + g c_N(N). \quad (18c)$$

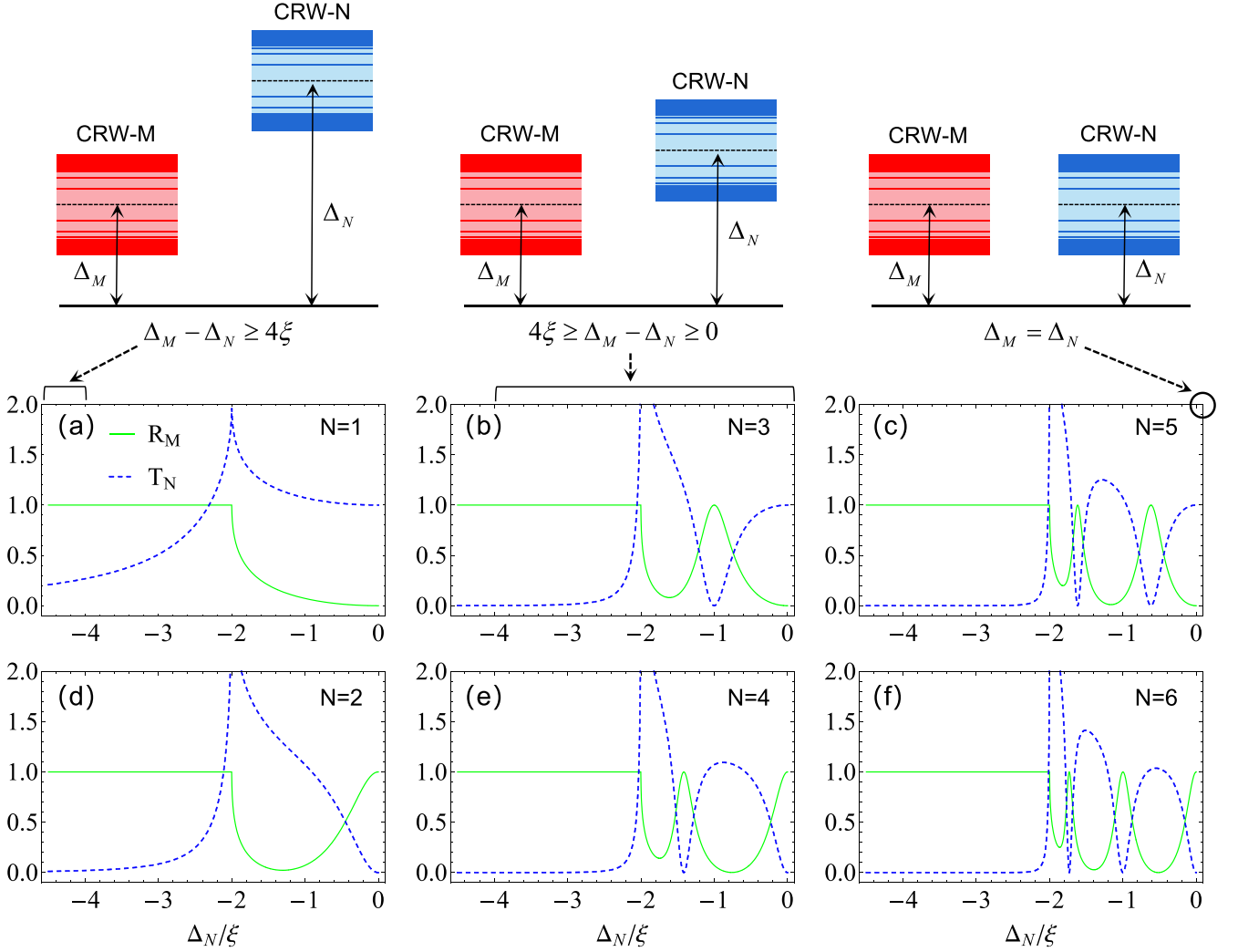


FIG. 10. The single-photon reflectance R_M (solid green line) and transfer rate T_N (blue dashed line) spectra are plotted as function of the detuning Δ_N . (a)–(c) and (d)–(f) corresponding to the case of $N = 1, 3, 5$ and $N = 2, 4, 6$, respectively. The spectrum are calculated for the parameters $g = 1\xi$, $\omega_M = \omega_e = 0$, $M = 1$.

The single-photon wave functions in the asymptotic regions and the continuous conditions of the system remain unchanged. Following the same solution steps in Sec. II, the transfer amplitude could be obtained. The same process can be extended to the case of giant atoms.

To simulate the transmission of the single photon across the entire bandwidth, we assume $k = q$ and $\omega_M = \omega_N + \omega_s$ in the following. The results are consistent with the cases in Sec. II. In Fig. 8, we plotted the transfer rate T_N as functions of the parameters M and N at the atom-waveguide resonance in the small atom system. The spectrum manifests that only when M and N are both odd values can a high transfer rate be achieved, confirming the previous conjecture in Sec. II A. We also explore the transmission rules in the giant atom system in Fig. 9. It can be observed that when the additional coupling locations are located at $4j - 2$ ($j = 1, 2, \dots$), the incident photon is completely reflected, even though the configuration allows full transmission in the small atom system for $M = N = 1$. For the case of $M = N = 2$ in Fig. 9(b), by choosing m and n to be both odd values, the original closed passage can be opened, confirming the previous conjecture in Sec. II B.

Additionally, Figs. 8 and 9(b) coincide; the extra coupling points of the giant atoms act in the same way as the single coupling point of the small atoms.

Now consider the more general case in small atom system, assume $\Delta_M = \omega_M - \omega_e$, $\Delta_N = \omega_N + \omega_s - \omega_e$. We calculate the transfer rate t_N under the condition of $\omega_M = \omega_e = 0$, there is

$$t_N = \frac{8i \sin\left(\frac{M\pi}{2}\right) \sin\left[N \arccos\left(\frac{\Delta_N}{2}\right)\right]}{\chi}, \quad (19)$$

the analytical expression guarantees that no photon is transmitted to CRW- N when the value of M is even. The variable χ represents a polynomial that does not impact the stated conclusion.

In Fig. 10, we have depicted the reflectance R_M and transfer rate T_N as functions of the detuning Δ_N at $E = 0$, accompanied by three distinct band configurations illustrated above the figures. When $\Delta_M - \Delta_N \geq 4\xi$, indicating complete separation of the two bands, the wave vector q becomes complex with a positive imaginary component. In the scenario where $N = 1$, we observe $T_N \neq 0$ due to the formation of a

stationary wave in the coupling resonator between CRW- N and the atom. Here, the bound states in CRW- N constitute the closed channel- N , with T_N representing both the amplitude of the bound states localized around the atom and the transmission coefficient. Conversely, for $N \geq 2$, single photons are localized around the atom, forming local modes in CRW- N , preventing the travel of single photons in CRW- N . For $4\xi \geq \Delta_M - \Delta_N \geq 0$, signifying partial overlap of the two bands, the figures illustrate that T_N can exceed 1 for the bound state of CRW- N . This intriguing phenomenon can be elucidated by the divergence of the scattering cross section when the energy of the incident particle aligns with the bound state of the closed channel, akin to the Feshbach resonance in cold atom scattering [66]. Moreover, when the energy bands of the two waveguides overlap by half, the transmission probability reaches its maximum. By comparing Figs. 10(a)–10(c) or Figs. 10(d)–10(f), we deduce that the enlargement of the stationary wave formation region solely increases the number of wave peaks. Finally, when $\Delta_M = \Delta_N$, corresponding to the perfect coincidence of the two bands, we have portrayed this scenario in Fig. 8.

IV. EXPERIMENTAL FEASIBILITY

In this section, we provide a detailed analysis of the experimental feasibility of this scheme. The CRW can be realized with at least three types of systems. (i) Defect resonators in photonic crystals: An array of photonic band gap cavities allows intercavity photon hopping due to their proximity and evanescent coupling between the cavities. The nitrogen vacancy (NV) diamond would be a candidate system, with the interesting transition at $637 \text{ nm} \approx 3 \times 10^{15} \text{ Hz}$ [67]. Silicon-on-silica photonic band gap cavities have achieved $Q \approx 10^7$ [68], meeting the requirements of the system for photon hopping between adjacent cavities. Additionally, adopting an asymmetric cavity [69] at the termination of the waveguide enables the construction of a semi-infinite dimensional waveguide. For instance, within a high-finesse Fabry-Pérot cavity measuring $335 \mu\text{m}$ in length, the decay rates of the cavity mirrors may be observed as $\kappa_1 = 2\pi \times 3.1 \text{ MHz}$ and $\kappa_2 = 2\pi \times 0.2 \text{ MHz}$ [70]. (ii) Coupled superconducting transmission line resonators: The traditional model of atom-cavity interaction can be represented by the coupling between line resonators and charge qubits [71]. We construct the configuration and take the length of line resonators $L = 1 \text{ cm}$, with the capacitance per unit length $C = 0.13 \text{ fF}/\mu\text{m}$ [72]. In addition, the charge qubit could be represented by a biased Cooper pair box (CPB) with a proper biased voltage V_g [73]. (iii) Atomic waveguides: Atomic waveguides are an intrinsically quantum reservoir, made of spins using an array of neutral atoms trapped in optical lattices [74,75] or tweezers [76–78]. Compared to conventional dielectric structures, the optical properties of atomic arrays can be dynamically controlled via external dressing fields.

In experiments on superconducting circuits, numerous studies have showcased the feasibility of fabricating LC circuit arrays [79,80]. The transmon qubit, acting as a giant atom, has been instrumental in establishing multiple coupling points to the flux line [37], as well as achieving qubit-qubit coupling [81–84]. Drawing upon these advancements in

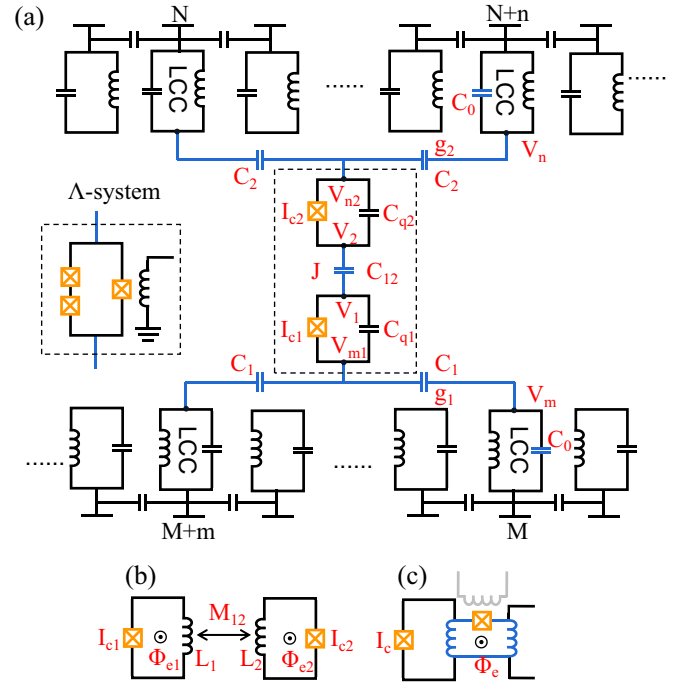


FIG. 11. Effective superconducting circuit diagram of the devices.

superconducting experiments, we have developed a concrete superconducting circuit, depicted in Fig. 11(a), where LC circuits (LCCs) function as resonators interconnected by capacitors. Within the enclosed area demarcated by a dotted box, two transmon qubits are coupled with a strength denoted as J . This coupling is achieved by inserting a capacitor C_{12} between the voltage nodes of the two circuits involved [56,85]. The transmission line establishes connections between the LCCs and the transmon qubit, characterized by coupling strengths g_i ($i = 1, 2$), modulated by capacitances C_i . The parameters adhere to certain constraints: $J \propto C_{12}V_1V_2 \propto C_{12}/C_{q1}C_{q2}$, $g_1 \propto C_1V_mV_{m1} \propto C_1/C_0C_{q1}$, and $g_2 \propto C_2V_nV_{n2} \propto C_2/C_0C_{q2}$, where C_0 denotes the coupling capacitance of the LCC, C_{q1} and C_{q2} represent the capacitance of the transmon qubits, C_{12} is the coupling capacitance between transmon qubits, and V_φ ($\varphi = 1, 2, m1, n2, m, n$) signifies the voltage operator of the corresponding voltage node being connected. Thus, by adjusting the coupling capacitances, we can attain the condition $g_1 = g_2 = J = g$. Moreover, it is feasible to employ qubit-qubit inductive coupling in Fig. 11(b) and qubit-waveguide inductive coupling in Fig. 11(c), where the coupling constants are controlled by external fields [85,86]. If we replace the two transmon qubits with a Λ system on the left, as proposed in Refs. [87–89], it could realize the configuration depicted in Fig. 7.

V. CONCLUSION

We conducted an analysis of the transmission properties of single photons in chiral and nonreciprocal modes within two distinct types of atom-CRW systems. The initial hybrid configuration involves two semi-infinite CRWs interconnected by two two-level atoms. In this scenario, a single photon undergoes elastic scattering, resulting in chiral transmission. Our

numerical simulations for a small atom system reveal that the transfer rate of incident photons is influenced by the coupling position between the atom and the waveguide (denoted as M and N), leading to either complete transfer or blockage. Specifically, our findings indicate that a high transfer rate is achievable at resonance only when both M and N are odd values. Upon extending our analysis to a giant atom system, we observed that additional coupling points (denoted as m and n) introduce unique interference effects, thereby revising the previous conclusions. Notably, in the case where M and N are not simultaneously odd values, the photon transfer channel is reopened. Conversely, the channel is closed when both M and N are odd values.

The second hybrid arrangement comprises two semi-infinite CRWs connected by a Λ -type atom. In this configuration, the transmission of a single photon undergoes an inelastic scattering process accompanied by frequency conversion, akin to the functionality of a single-photon diode. The direction of conduction is contingent upon the initial state of the atom. When a single photon with a wave vector k approaches from the left side of CRW- M , with the atom initially in state $|g\rangle$, it undergoes frequency conversion to q . Conversely, if the same single photon approaches from the right side of CRW- N and the atom is prepared in state $|s\rangle$, the frequency conversion results in $k \rightarrow q'$. The roles of the parameters M , N , m , n align with the scenarios observed in the two two-level atom system.

It is noteworthy that replacing the semi-infinite CRW with an infinite one is feasible, albeit resulting in a considerable reduction in the transfer rate (refer to Appendix). In essence, our research has revealed novel phenomena and applications within atom-CRW systems. These proposed systems seamlessly integrate nonreciprocity and the realm of giant atomic physics, presenting promising solutions for quantum network engineering and quantum information processing.

ACKNOWLEDGMENT

This work is supported by the National Natural Science Foundation of China under Grant No. 12375018.

APPENDIX: ONE CONFIGURATION COMBINING ONE SEMI-INFINITE CRW AND ONE INFINITE CRW

In this Appendix, we extend the semi-infinite lower bus waveguide in Fig. 1 to an infinite one. The Hamiltonian for the CRWs is written as

$$\begin{aligned}
 H'_w = & \sum_{j=-\infty}^{+\infty} \{ \omega_M a_M^\dagger(j) a_M(j) \\
 & - \xi [a_M^\dagger(j+1) a_M(j) + a_M^\dagger(j) a_M(j+1)] \\
 & + \sum_{j=1}^{+\infty} \{ \omega_N a_N^\dagger(j) a_N(j) \\
 & - \xi [a_N^\dagger(j+1) a_N(j) + a_N^\dagger(j) a_N(j+1)] \}, \quad (\text{A1})
 \end{aligned}$$

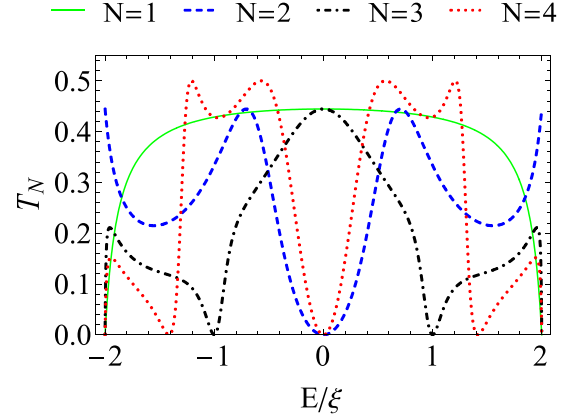


FIG. 12. The single-photon transfer rate T_N spectrum is plotted as a function of the incident energy E . There are four different values of N , in which $N = 1$ (solid green line), $N = 2$ (blue dashed line), $N = 3$ (black dot-dashed line), $N = 4$ (red dashed line). The spectrum is calculated for the parameters $g = 1\xi$, $\omega_M = \omega_N = \omega_1 = \omega_2 = 0$, $M = 0$.

then we have the Hamiltonian of the whole system $H' = H_a + H'_w + H_{\text{int}}$. In this small atom-waveguide system, we consider $M = 0$ as the coupling point in waveguide M .

The wave functions in the asymptotic regions are given, respectively, by

$$c_M(j) = \begin{cases} e^{-ikj} + r_M e^{ikj}, & j > 0 \\ t_M e^{-ikj}, & j < 0 \end{cases} \quad (\text{A2})$$

and

$$c_N(j) = \begin{cases} t_N e^{ikj}, & j > N \\ A \sin(kj), & j = 1, 2, \dots, N \end{cases} \quad (\text{A3})$$

where t_M is the transfer amplitude in the CRW- M . Together with the continuous condition at $j = 0, N$, which are

$$1 + r_M = t_M, \quad (\text{A4a})$$

$$t_N e^{ikN} = A \sin(kN). \quad (\text{A4b})$$

Finally, we obtain the analytic solution of transfer amplitude t_N as

$$t_N = \frac{2ie^{-ik}(e^{2ik} - 1)\sin(kN)}{\eta' - 4iE\sin(k) + e^{2ikN}[2iE\sin(k) - 1]}, \quad (\text{A5})$$

where $\eta' = 3 - 2E^2 + 2(E^2 - 1)\cos(2k)$.

In Fig. 12, we present the transfer rate T_N as a function of the incident energy E , where the coupling point in CRW- N is varied from 1 to 4. The spectrum reveals that a high transfer rate is only attainable around $E = 0$ when N is an odd value. In comparison to the scenario in Sec. II, more than half of the probability indicates that the single photon will be reflected and transmitted in CRW- M throughout the entire bandwidth. Consequently, the transfer rate T_N in this configuration is limited to no more than 0.5.

- [1] C. Genes, A. Mari, D. Vitali, and P. Tombesi, Quantum effects in optomechanical systems, *Adv. At. Mol. Opt. Phys.* **57**, 33 (2009).
- [2] G. S. Agarwal and S. Huang, Optomechanical systems as single-photon routers, *Phys. Rev. A* **85**, 021801(R) (2012).
- [3] W. H. P. Nielsen, Y. Tsaturyan, C. B. Møller, E. S. Polzik, and A. Schliesser, Multimode optomechanical system in the quantum regime, *Proc. Natl. Acad. Sci. USA* **114**, 62 (2017).
- [4] Z.-L. Xiang, S. Ashhab, J. Q. You, and F. Nori, Hybrid quantum circuits: Superconducting circuits interacting with other quantum systems, *Rev. Mod. Phys.* **85**, 623 (2013).
- [5] D.-W. Zhang, Y.-Q. Zhu, Y. Zhao, H. Yan, and S.-L. Zhu, Topological quantum matter with cold atoms, *Adv. Phys.* **67**, 253 (2018).
- [6] S. Chu, Cold atoms and quantum control, *Nature (London)* **416**, 206 (2002).
- [7] S. Haroche and D. Kleppner, Cavity quantum electrodynamics, *Phys. Today* **42**(1), 24 (1989).
- [8] H. Mabuchi and A. Doherty, Cavity quantum electrodynamics: coherence in context, *Science* **298**, 1372 (2002).
- [9] H. Walther, B. T. Varcoe, B.-G. Englert, and T. Becker, Cavity quantum electrodynamics, *Rep. Prog. Phys.* **69**, 1325 (2006).
- [10] A. Blais, S. M. Girvin, and W. D. Oliver, Quantum information processing and quantum optics with circuit quantum electrodynamics, *Nature Phys.* **16**, 247 (2020).
- [11] S. Haroche, M. Brune, and J. Raimond, From cavity to circuit quantum electrodynamics, *Nature Phys.* **16**, 243 (2020).
- [12] A. Blais, A. L. Grimsmo, S. M. Girvin, and A. Wallraff, Circuit quantum electrodynamics, *Rev. Mod. Phys.* **93**, 025005 (2021).
- [13] H. Zheng, D. J. Gauthier, and H. U. Baranger, Waveguide-qed-based photonic quantum computation, *Phys. Rev. Lett.* **111**, 090502 (2013).
- [14] K. Lalumiere, B. C. Sanders, A. F. van Loo, A. Fedorov, A. Wallraff, and A. Blais, Input-output theory for waveguide QED with an ensemble of inhomogeneous atoms, *Phys. Rev. A* **88**, 043806 (2013).
- [15] D. Roy, C. M. Wilson, and O. Firstenberg, Colloquium: Strongly interacting photons in one-dimensional continuum, *Rev. Mod. Phys.* **89**, 021001 (2017).
- [16] X. Gu, A. F. Kockum, A. Miranowicz, Y.-X. Liu, and F. Nori, Microwave photonics with superconducting quantum circuits, *Phys. Rep.* **718–719**, 1 (2017).
- [17] A. Yariv, Y. Xu, R. K. Lee, and A. Scherer, Coupled-resonator optical waveguide: A proposal and analysis, *Opt. Lett.* **24**, 711 (1999).
- [18] S. Mookherjea and A. Yariv, Coupled resonator optical waveguides, *IEEE J. Sel. Top. Quantum Electron.* **8**, 448 (2002).
- [19] P.-B. Li, Y. Gu, Q.-H. Gong, and G.-C. Guo, Quantum-information transfer in a coupled resonator waveguide, *Phys. Rev. A* **79**, 042339 (2009).
- [20] K. Y. Bliokh, Y. P. Bliokh, V. Freilikher, S. Savel'ev, and F. Nori, Colloquium: Unusual resonators: Plasmonics, metamaterials, and random media, *Rev. Mod. Phys.* **80**, 1201 (2008).
- [21] L. Zhou, L.-P. Yang, Y. Li, and C. P. Sun, Quantum routing of single photons with a cyclic three-level system, *Phys. Rev. Lett.* **111**, 103604 (2013).
- [22] J.-S. Huang, J.-W. Wang, Y. Wang, Y.-L. Li, and Y.-W. Huang, Control of single-photon routing in a t-shaped waveguide by another atom, *Quantum Inf. Process.* **17**, 1 (2018).
- [23] F. Morichetti, C. Ferrari, A. Canciamilla, and A. Melloni, The first decade of coupled resonator optical waveguides: bringing slow light to applications, *Laser Photon. Rev.* **6**, 74 (2012).
- [24] L. Zhou, Y. B. Gao, Z. Song, and C. P. Sun, Coherent output of photons from coupled superconducting transmission line resonators controlled by charge qubits, *Phys. Rev. A* **77**, 013831 (2008).
- [25] G. Calajó, F. Ciccarello, D. Chang, and P. Rabl, Atom-field dressed states in slow-light waveguide qed, *Phys. Rev. A* **93**, 033833 (2016).
- [26] H. Zheng and H. U. Baranger, Persistent quantum beats and long-distance entanglement from waveguide-mediated interactions, *Phys. Rev. Lett.* **110**, 113601 (2013).
- [27] W. Healy, Comment on “electric dipole interaction in quantum optics”, *Phys. Rev. A* **22**, 2891 (1980).
- [28] T. Takagi, M. Wakayama, K. Tanaka, N. Kunihiro, K. Kimoto, and Y. Ikematsu, *International Symposium on Mathematics, Quantum Theory, and Cryptography: Proceedings of MQC 2019* (Springer Nature, Berlin, 2021).
- [29] C. Joshi, F. Yang, and M. Mirhosseini, Resonance fluorescence of a chiral artificial atom, *Phys. Rev. X* **13**, 021039 (2023).
- [30] M. V. Gustafsson, T. Aref, A. F. Kockum, M. K. Ekström, G. Johansson, and P. Delsing, Propagating phonons coupled to an artificial atom, *Science* **346**, 207 (2014).
- [31] K. J. Satzinger, Y. Zhong, H.-S. Chang, G. A. Peairs, A. Bienfait, M.-H. Chou, A. Cleland, C. R. Conner, É. Dumur, J. Grebel *et al.*, Quantum control of surface acoustic-wave phonons, *Nature (London)* **563**, 661 (2018).
- [32] G. Andersson, M. K. Ekström, and P. Delsing, Electromagnetically induced acoustic transparency with a superconducting circuit, *Phys. Rev. Lett.* **124**, 240402 (2020).
- [33] A. Frisk Kockum, P. Delsing, and G. Johansson, Designing frequency-dependent relaxation rates and lamb shifts for a giant artificial atom, *Phys. Rev. A* **90**, 013837 (2014).
- [34] A. M. Vadiraj, A. Ask, T. G. McConkey, I. Nsanzineza, C. W. Sandbo Chang, A. F. Kockum, and C. M. Wilson, Engineering the level structure of a giant artificial atom in waveguide quantum electrodynamics, *Phys. Rev. A* **103**, 023710 (2021).
- [35] L. Guo, A. Grimsmo, A. F. Kockum, M. Pletyukhov, and G. Johansson, Giant acoustic atom: A single quantum system with a deterministic time delay, *Phys. Rev. A* **95**, 053821 (2017).
- [36] A. Ask, M. Ekström, P. Delsing, and G. Johansson, Cavity-free vacuum-rabi splitting in circuit quantum acoustodynamics, *Phys. Rev. A* **99**, 013840 (2019).
- [37] B. Kannan, M. J. Ruckriegel, D. L. Campbell, A. Frisk Kockum, J. Braumüller, D. K. Kim, M. Kjaergaard, P. Krantz, A. Melville, B. M. Niedzielski *et al.*, Waveguide quantum electrodynamics with superconducting artificial giant atoms, *Nature (London)* **583**, 775 (2020).
- [38] A. F. Kockum, G. Johansson, and F. Nori, Decoherence-free interaction between giant atoms in waveguide quantum electrodynamics, *Phys. Rev. Lett.* **120**, 140404 (2018).
- [39] L. Guo, A. F. Kockum, F. Marquardt, and G. Johansson, Oscillating bound states for a giant atom, *Phys. Rev. Res.* **2**, 043014 (2020).
- [40] S. Guo, Y. Wang, T. Purdy, and J. Taylor, Beyond spontaneous emission: Giant atom bounded in the continuum, *Phys. Rev. A* **102**, 033706 (2020).

- [41] D.-W. Wang, H.-T. Zhou, M.-J. Guo, J.-X. Zhang, J. Evers, and S.-Y. Zhu, Optical diode made from a moving photonic crystal, *Phys. Rev. Lett.* **110**, 093901 (2013).
- [42] K. Xia, M. Alamri, and M. S. Zubairy, Ultrabroadband non-reciprocal transverse energy flow of light in linear passive photonic circuits, *Opt. Express* **21**, 25619 (2013).
- [43] P. Lodahl, S. Mahmoodian, S. Stobbe, A. Rauschenbeutel, P. Schneeweiss, J. Volz, H. Pichler, and P. Zoller, Chiral quantum optics, *Nature (London)* **541**, 473 (2017).
- [44] Y. Tokura and N. Nagaosa, Nonreciprocal responses from non-centrosymmetric quantum materials, *Nat. Commun.* **9**, 3740 (2018).
- [45] L. Tang, J. Tang, W. Zhang, G. Lu, H. Zhang, Y. Zhang, K. Xia, and M. Xiao, On-chip chiral single-photon interface: Isolation and unidirectional emission, *Phys. Rev. A* **99**, 043833 (2019).
- [46] X.-Y. Yao, H. Ali, F.-L. Li, and P.-B. Li, Nonreciprocal phonon blockade in a spinning acoustic ring cavity coupled to a two-level system, *Phys. Rev. Appl.* **17**, 054004 (2022).
- [47] J.-C. Zheng and P.-B. Li, Few-photon isolation in a one-dimensional waveguide using chiral quantum coupling, *Opt. Express* **31**, 21881 (2023).
- [48] C.-P. Shen, J.-Q. Chen, X.-F. Pan, Y.-M. Ren, X.-L. Dong, X.-L. Hei, Y.-F. Qiao, and P.-B. Li, Tunable nonreciprocal photon correlations induced by directional quantum squeezing, *Phys. Rev. A* **108**, 023716 (2023).
- [49] R. Riedinger, S. Hong, R. A. Norte, J. A. Slater, J. Shang, A. G. Krause, V. Anant, M. Aspelmeyer, and S. Gröblacher, Non-classical correlations between single photons and phonons from a mechanical oscillator, *Nature (London)* **530**, 313 (2016).
- [50] A. C. Mahoney, J. I. Colless, S. J. Pauka, J. M. Hornibrook, J. D. Watson, G. C. Gardner, M. J. Manfra, A. C. Doherty, and D. J. Reilly, On-chip microwave quantum hall circulator, *Phys. Rev. X* **7**, 011007 (2017).
- [51] K. Xia, G. Lu, G. Lin, Y. Cheng, Y. Niu, S. Gong, and J. Twamley, Reversible nonmagnetic single-photon isolation using unbalanced quantum coupling, *Phys. Rev. A* **90**, 043802 (2014).
- [52] K. Xia, F. Nori, and M. Xiao, Cavity-free optical isolators and circulators using a chiral cross-kerr nonlinearity, *Phys. Rev. Lett.* **121**, 203602 (2018).
- [53] F. Lecocq, F. Quinlan, K. Cicak, J. Aumentado, S. Diddams, and J. Teufel, Control and readout of a superconducting qubit using a photonic link, *Nature (London)* **591**, 575 (2021).
- [54] L. Du, Y.-T. Chen, and Y. Li, Nonreciprocal frequency conversion with chiral λ -type atoms, *Phys. Rev. Res.* **3**, 043226 (2021).
- [55] J. Zhou, X.-L. Yin, and J.-Q. Liao, Chiral and nonreciprocal single-photon scattering in a chiral-giant-molecule waveguide-QED system, *Phys. Rev. A* **107**, 063703 (2023).
- [56] S. Filipp, M. Göppl, J. M. Fink, M. Baur, R. Bianchetti, L. Steffen, and A. Wallraff, Multimode mediated qubit-qubit coupling and dark-state symmetries in circuit quantum electrodynamics, *Phys. Rev. A* **83**, 063827 (2011).
- [57] L. Zhou, Z. R. Gong, Y.-X. Liu, C. P. Sun, and F. Nori, Controllable scattering of a single photon inside a one-dimensional resonator waveguide, *Phys. Rev. Lett.* **101**, 100501 (2008).
- [58] M. Ahumada, P. A. Orellana, F. Domínguez-Adame, and A. V. Malyshev, Tunable single-photon quantum router, *Phys. Rev. A* **99**, 033827 (2019).
- [59] X. Wang and H.-R. Li, Chiral quantum network with giant atoms, *Quantum Sci. Technol.* **7**, 035007 (2022).
- [60] W. Zhao and Z. Wang, Single-photon scattering and bound states in an atom-waveguide system with two or multiple coupling points, *Phys. Rev. A* **101**, 053855 (2020).
- [61] J. T. Shen and S. Fan, Coherent photon transport from spontaneous emission in one-dimensional waveguides, *Opt. Lett.* **30**, 2001 (2005).
- [62] G. Zumofen, N. M. Mojarad, V. Sandoghdar, and M. Agio, Perfect reflection of light by an oscillating dipole, *Phys. Rev. Lett.* **101**, 180404 (2008).
- [63] D. Witthaut and A. S. Sørensen, Photon scattering by a three-level emitter in a one-dimensional waveguide, *New J. Phys.* **12**, 043052 (2010).
- [64] D. Pinotsi and A. Imamoglu, Single photon absorption by a single quantum emitter, *Phys. Rev. Lett.* **100**, 093603 (2008).
- [65] C. Gonzalez-Ballester, E. Moreno, F. J. Garcia-Vidal, and A. Gonzalez-Tudela, Nonreciprocal few-photon routing schemes based on chiral waveguide-emitter couplings, *Phys. Rev. A* **94**, 063817 (2016).
- [66] P. Courteille, R. S. Freeland, D. J. Heinzen, F. A. Van Abeelen, and B. J. Verhaar, Observation of a Feshbach resonance in cold atom scattering, *Phys. Rev. Lett.* **81**, 69 (1998).
- [67] A. D. Greentree, C. Tahan, J. H. Cole, and L. C. Hollenberg, Quantum phase transitions of light, *Nat. Phys.* **2**, 856 (2006).
- [68] B.-S. Song, S. Noda, T. Asano, and Y. Akahane, Ultra-high-Q photonic double-heterostructure nanocavity, *Nat. Mater.* **4**, 207 (2005).
- [69] X. Xia, J. Xu, and Y. Yang, Controllable optical bistability of an asymmetric cavity containing a single two-level atom, *Phys. Rev. A* **90**, 043857 (2014).
- [70] P. Yang, X. Xia, H. He, S. Li, X. Han, P. Zhang, G. Li, P. Zhang, J. Xu, Y. Yang *et al.*, Realization of nonlinear optical nonreciprocity on a few-photon level based on atoms strongly coupled to an asymmetric cavity, *Phys. Rev. Lett.* **123**, 233604 (2019).
- [71] Y. A. Pashkin, T. Yamamoto, O. Astafiev, Y. Nakamura, D. Averin, and J. Tsai, Quantum oscillations in two coupled charge qubits, *Nature (London)* **421**, 823 (2003).
- [72] A. Wallraff, D. I. Schuster, A. Blais, L. Frunzio, R.-S. Huang, J. Majer, S. Kumar, S. M. Girvin, and R. J. Schoelkopf, Strong coupling of a single photon to a superconducting qubit using circuit quantum electrodynamics, *Nature (London)* **431**, 162 (2004).
- [73] Y. Nakamura, Y. A. Pashkin, and J. Tsai, Coherent control of macroscopic quantum states in a single-cooper-pair box, *Nature (London)* **398**, 786 (1999).
- [74] J. Zeiher, P. Schauß, S. Hild, T. Macrì, I. Bloch, and C. Gross, Microscopic characterization of scalable coherent rydberg superatoms, *Phys. Rev. X* **5**, 031015 (2015).
- [75] T. Weber, M. Hönig, T. Niederprüm, T. Manthey, O. Thomas, V. Guarrera, M. Fleischhauer, G. Barontini, and H. Ott, Mesoscopic Rydberg-blockaded ensembles in the superatom regime and beyond, *Nature Phys.* **11**, 157 (2015).
- [76] M. Schlosser, J. Kruse, C. Gierl, S. Teichmann, S. Tichelmann, and G. Birkl, Fast transport, atom sample splitting and single-atom qubit supply in two-dimensional arrays of optical microtraps, *New J. Phys.* **14**, 123034 (2012).
- [77] A. M. Hankin, Y.-Y. Jau, L. P. Parazzoli, C. W. Chou, D. J. Armstrong, A. J. Landahl, and G. W. Biedermann, Two-atom Rydberg blockade using direct $6S$ to nP excitation, *Phys. Rev. A* **89**, 033416 (2014).

- [78] K. M. Maller, M. T. Lichtman, T. Xia, Y. Sun, M. J. Piotrowicz, A. W. Carr, L. Isenhower, and M. Saffman, Rydberg-blockade controlled-not gate and entanglement in a two-dimensional array of neutral-atom qubits, *Phys. Rev. A* **92**, 022336 (2015).
- [79] Y. Li, Y. Sun, W. Zhu, Z. Guo, J. Jiang, T. Kariyado, H. Chen, and X. Hu, Topological LC-circuits based on microstrips and observation of electromagnetic modes with orbital angular momentum, *Nat. Commun.* **9**, 4598 (2018).
- [80] T. Helbig, T. Hofmann, S. Imhof, M. Abdelghany, T. Kiessling, L. Molenkamp, C. Lee, A. Szameit, M. Greiter, and R. Thomale, Generalized bulk–boundary correspondence in non-hermitian topoelectrical circuits, *Nat. Phys.* **16**, 747 (2020).
- [81] T. Hime, P. Reichardt, B. Plourde, T. Robertson, C.-E. Wu, A. Ustinov, and J. Clarke, Solid-state qubits with current-controlled coupling, *Science* **314**, 1427 (2006).
- [82] A. Niskanen, K. Harrabi, F. Yoshihara, Y. Nakamura, S. Lloyd, and J. S. Tsai, Quantum coherent tunable coupling of superconducting qubits, *Science* **316**, 723 (2007).
- [83] J. Plantenberg, P. De Groot, C. Harmans, and J. Mooij, Demonstration of controlled-not quantum gates on a pair of superconducting quantum bits, *Nature (London)* **447**, 836 (2007).
- [84] J. Majer, J. Chow, J. Gambetta, J. Koch, B. Johnson, J. Schreier, L. Frunzio, D. Schuster, A. A. Houck, A. Wallraff *et al.*, Coupling superconducting qubits via a cavity bus, *Nature (London)* **449**, 443 (2007).
- [85] P. Krantz, M. Kjaergaard, F. Yan, T. P. Orlando, S. Gustavsson, and W. D. Oliver, A quantum engineer’s guide to superconducting qubits, *Appl. Phys. Rev.* **6**, 021318 (2019).
- [86] L. Du, Y.-T. Chen, Y. Zhang, and Y. Li, Giant atoms with time-dependent couplings, *Phys. Rev. Res.* **4**, 023198 (2022).
- [87] K. Koshino, K. Inomata, T. Yamamoto, and Y. Nakamura, Implementation of an impedance-matched Λ system by dressed-state engineering, *Phys. Rev. Lett.* **111**, 153601 (2013).
- [88] K. Inomata, K. Koshino, Z. R. Lin, W. D. Oliver, J. S. Tsai, Y. Nakamura, and T. Yamamoto, Microwave down-conversion with an impedance-matched Λ system in driven circuit QED, *Phys. Rev. Lett.* **113**, 063604 (2014).
- [89] K. Inomata, Z. Lin, K. Koshino, W. D. Oliver, J.-S. Tsai, T. Yamamoto, and Y. Nakamura, Single microwave-photon detector using an artificial λ -type three-level system, *Nat. Commun.* **7**, 12303 (2016).